An Integrated AFM and SANS Approach toward Understanding Void Formation in Conductive Composite Materials

J. Oakey and D. W. M. Marr*

Chemical Engineering Department, Colorado School of Mines, Golden, Colorado 80401

K. B. Schwartz and M. Wartenberg

Tyco Electronics Corporation, 300 Constitution Dr., Menlo Park, California 94025

Received January 3, 2000; Revised Manuscript Received April 19, 2000

ABSTRACT: The morphology of voids within carbon black-filled polyethylene conductive composites has been studied by both atomic force microscopy and small-angle neutron scattering. Both void size and polyethylene crystalline lamellae thickness were measured with both techniques, and the results were compared. Atomic force micrographs indicate that voids form at the carbon black−polyethylene interface as previously hypothesized from the interpretation of neutron scattering experiments alone. This result supports the conclusion that voids provide a stress release mechanism during polyethylene crystallization and that variables such as filler morphology, volume fraction, and polymer crystallinity may be used to quantitatively predict the extent of void incorporation as composite composition is varied.

Introduction

Carbon black-filled polyethylene composites have been the focus of much research attention in recent years because of the strong dependence of mechanical and electrical properties on composite morphology.[1−6] This system exhibits a positive temperature coefficient (PTC) effect,[5,7,8] where composite resistivity can be a very strong function of temperature and is used as self-regulating heaters and resettable fuses.[9,10] Because of this system's commercial importance, its microstructure has been extensively examined by various scattering and microscopy techniques.[1,6,8,11,12] Although a variety of techniques have been applied, questions remain concerning the mechanisms of morphology development during the processing of these composites. For example, despite their important role in composite function, the formation and structure of voids have not been thoroughly studied. Here, we focus our attention on a new combination of techniques to investigate the mechanisms of void formation during the processing of carbon black-filled polyethylene composites.

Voids in these materials were first detected through comparison of small-angle neutron and X-ray scattering (SANS and SAXS) experiments and quantitatively confirmed by pycnometry.[1] Subsequently, a formalism was developed which enables the quantification of void size and volume fraction in bulk composites.[11] This method uses SANS alone and relies upon the comparison of SANS profiles from multiple composites separately formulated with protonated and deuterated polyethylene (hPE and dPE). The sensitivity of SANS to isotopic substitution makes it an ideal technique for discriminating and measuring the bulk void phase in these conductive composite materials.

Subsequent work has employed the same method of SANS contrast variation to investigate the void phase in composites of varying polymer and filler morphology.[12] This study demonstrated an empirical relationship between the volume fraction of the void phase and filler surface area, suggesting that voids form as a result of interfacial composite morphology, an interpretation reinforced by the observation that voids are not present at temperatures above the melting point of polyethylene. Presumably, these voids result from stress generated by the crystallizing polymer matrix during composite processing.

The neutron scattering/contrast matching approach, however, is sensitive only to bulk morphology and is incapable of identifying the specific location of void development. Whether voids form at the carbon black−polyethylene interface or within the polyethylene matrix may have a strong effect upon electrical performance because conductivity through the material occurs as a result of tunneling between adjacent particles in the matrix.[1] Voids at these junctures could lead to decreased performance, reliability, or catastrophic failure. To complement our SANS studies and identify the deducing and mechanisms of void formation, we require a technique that provides specific information regarding local morphology. It has been shown that a variation of Tapping Mode atomic force microscopy (AFM) known as phase imaging is capable of imaging the nanostructure of blended or multiphase materials with high resolution at submicron length scales.[13,14] Using SANS, we have previously observed voids in a size range between 50 and 250 nm in size;[12] therefore, AFM should be an appropriate technique for directly observing the void phase in carbon black−polyethylene composites.

AFM has previously been utilized to study several aspects of filled polymer composites such as particle microdispersion,[15] fiber−polymer interfacial morphology,[16] polymer blend crystal morphology,[17] and composite deformation under shear.[18] In this work we employ AFM to obtain both topography and phase images of conductive composites. Complementary information is obtained through the combination of these modes that allow for comparison of AFM data to SANS results as well as the direct investigation of carbon black−polyethylene interfaces. In this manner we connect the current AFM study with previous SANS investigations to identify the mechanism of void morphology development in these materials.

10.1021/ma0000024 CCC: $19.00
Published on Web 06/23/2000

Table 1. Average Void Size for Different Carbon Black Morphologies

carbon black structure	CB primary particle size (nm)[34]	CB primary aggregate size (nm)[34]	void size (nm) from SANS	void size (nm) from AFM
low	56	134	242 ± 40	247 ± 14
medium	82	204	47 ± 30	70 ± 16
high	95	670	41 ± 10	62 ± 19

Experimental Approach

Sample Preparation. Experiments were conducted with composites of carbon black volume fractions ranging from 0.085 to 0.429 using a lamp black of high structure and furnace blacks of medium and low structure[12] (see Table 1). Each carbon black at a particular volume fraction was separately compounded into hPE and dPE for void measurements via SANS. Composites were prepared in a DACA small-scale twin-screw minicompounder,[19] a mixer/extruder designed for formulations of 1−5 cm^3. Carbon black was added to each polyethylene to achieve the appropriate volumetric composition at a constant total mass of 3 g and mixed at 190 °C and 100 rpm for 5 min in the minicompounder.

From the extruded composite material, 76.2 × 76.2 mm^2 slabs were pressed at 205 °C under 44 482 N to a thickness of 0.356 mm using a hydraulic press. These slabs were then inserted into another press at the same pressure and brought to 25 °C with cooling water in order to expedite the cooling process at the press pressure. The slabs were subsequently punched into 16 mm diameter disks and annealed by heating from room temperature to 170 °C at a rate of 2 °C/min under atmospheric pressure and composition. We selected 170 °C as an annealing temperature because it is high enough to remove the thermal history of the polymer, yet low enough to prevent significant oxidation.[20] Additionally, it has been demonstrated that carbon black serves to significantly suppress thermal oxidation in polyethylenes even at low weight fractions.[21−23] After being held for 90 min at 170 °C the samples were first brought to 100 °C at 0.5 °C/min and then to room temperature at 2 °C/min.

Samples were prepared from these slabs for AFM characterization by cutting an approximately 2 × 2 mm^2 section from the slab with a razor blade. This small sample was then imbedded in an epoxy (bisphenol A (epichlorhydrine)) mold to facilitate microtoming of the composite face. Microtoming produced thinly sliced composite slices (<25 μm) which were analyzed by AFM. Inspection of initial AFM images revealed the effects of microtoming on the sample surface. To remove such artifacts and achieve morphology similar to that imparted by the original annealing cycle, the samples were once again annealed using a high-temperature AFM stage (Digital Instruments, Santa Barbara, CA). Due to the limitations of the stage (T_{max} = 120 °C), the original heating cycle was approximated as closely as possible. The sample was heated from 25 to 120 °C at a rate of 2 °C/min and held for 2 h, at which point they were brought to 85 °C at 1 °C/min and then returned to 25 °C

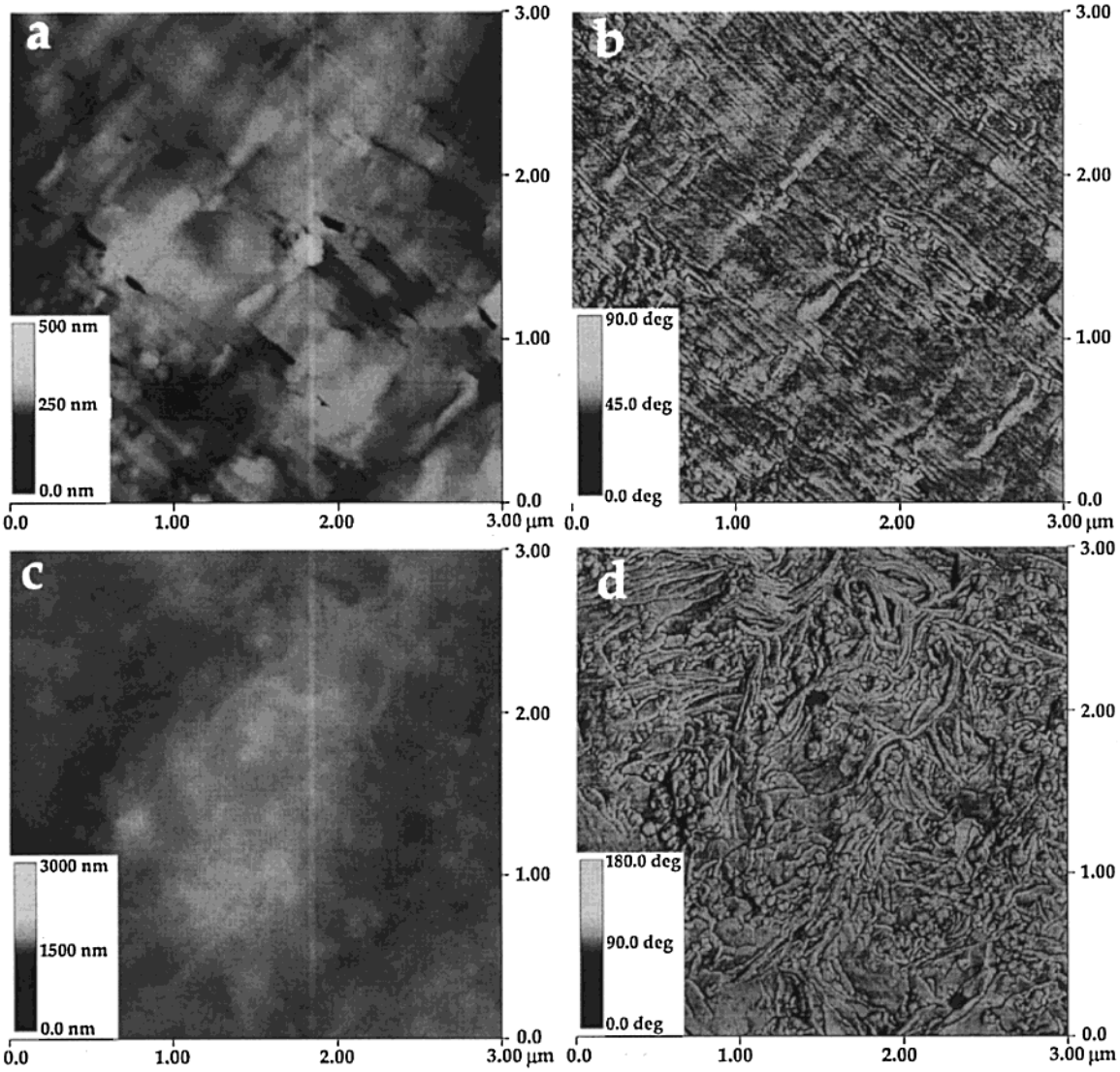

Figure 1. 36% carbon black-filled dPE after microtoming (a, b) and after subsequent annealing (c, d). Tapping mode AFM height (a, c) and phase (b, d) images are shown.

at 2 °C/min. AFM images of the postannealed composite samples showed no remnants of the microtoming process.

Small-Angle Neutron Scattering (SANS). Scattering experiments were performed on the 30 m SANS beamline (NG-7) at the National Institute of Standards and Technology Center for Neutron Research in Gaithersburg, MD. The incident neutron beam of wavelength 5 Å was collimated by source and sample slits separated by a distance of 7.5 m. The sample−detector distance was 17.5 m, providing an effective q range of 0.002 $nm^{-1} < q < 0.4864$ nm^{-1}. Over the entire q range, all scattering data were corrected on a cell by cell basis for instrumental backgrounds and detector efficiency variation, divided by the sample transmission and thickness and normalized to a constant incident flux. The net intensities were converted to an absolute differential scattering cross section, $[d\Sigma/d\Omega(q)]$, per unit sample volume (in units of cm^{-1}) via precalibrated secondary standards.[24] Incoherent scattering, due primarily to protons in the hPE, was calculated and subtracted according to a procedure described previously.[25] The analytical procedure to determine void size and volume fraction from reduced SANS data has been described previously.[12]

Atomic Force Microscopy (AFM). AFM experiments were performed on a Nanoscope IIIa, multimode (Digital Instruments, Santa Barbara, CA) equipped with an extender electronics module. Both topography and phase images were collected using tapping mode in air at room temperature. Measurements of lamellar thickness and void size were performed using section analysis on Digital Instrument's AFM analysis software package. Repeated measurements were averaged, and the standard deviation was calculated. As the feature size being measured was larger than the probe dimensions in the x and y directions and significantly smaller along the z-axis, no deconvolution was required to correct for tip effects in the atomic force micrographs before measuring lamellar widths.[26,27]

Results and Discussion

AFM images of a freshly microtomed composite and the same composite immediately after heater stage annealing are shown in Figure 1. It is evident that post-microtome annealing is effective at removing shear-induced orientation at the sample surface. In these images, the benefit of phase imaging is also apparent. Specific composite features such as polyethylene lamellae and carbon black aggregates can be distinguished in height mode; however, the phase images are much clearer and remove artifacts due to surface roughness which could skew size or position analysis. We therefore use phase imaging to determine whether the composite has regained morphology typical of the bulk, specifically by comparing lamellae thickness, a feature measurable by both SANS and AFM. Though phase imaging highlights the location of interfaces within the composite, it cannot be used to locate or identify voids, which do not appear in this mode. Height mode is therefore used in combination with phase imaging to detect sudden discontinuities in topography along the correct length scales, which we interpret as voids.

Figure 2a shows typical SANS profiles for carbon black-filled hPE and dPE. Also shown is the hPE-filled composite profile that has been divided by the scattering invariant ratio[12] in order to normalize for the contrast difference between hPE and dPE. Deviations of this curve from the dPE-filled composite represent morphological features that are not apparent in hPE-filled composites, namely voids and the crystalline lamellae phase. Subtracting the dPE composite curve from the hPE composite curve, as shown in Figure 2b, highlights these features and allows for easier quantification. We measure the second peak, the crystalline lamellae long spacing Bragg peak, by first dividing by a correction factor to account for the unoriented state of lamellae.[28,29] The correction for the Lorentz and polarization factors is given by

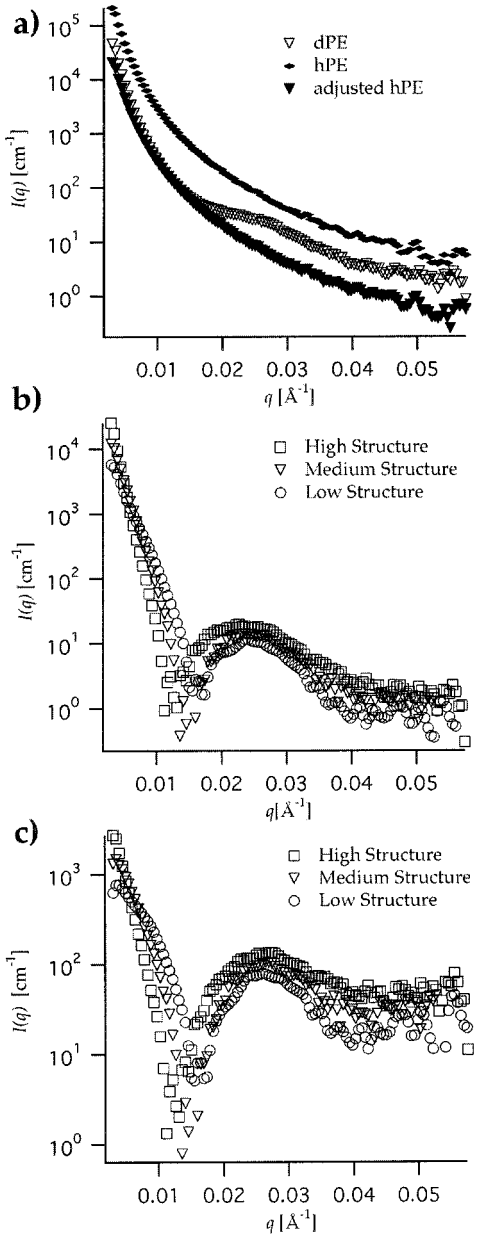

Figure 2. (a) Typical SANS data from carbon black-filled hPE and dPE composites. The second hPE curve has been normalized for SANS contrast. (b) Uncorrected and (c) Lorentz corrected data. The first peak is attributable to the void phase, while the second peak is the crystalline lamellae long spacing Bragg peak.

$$Lp = \frac{1 + \cos^2 2\theta}{\sin^2 \theta \cos \theta}$$

and is appropriate for perfectly random crystals in a disk or rod geometry.[30] Once the long spacing Bragg peak position has been established, the mean lamellar thickness (L_m) may be calculated by

$$L_m = X_c L_c$$

where L_c is the long spacing obtained from Bragg's law. X_c, the weight percent of crystalline polymer in the

Table 2. Polyethylene Lamellae Width for 36 Volume % Carbon Black Composites

carbon black structure	X_c (wt %)	L_m (nm) from SANS	L_m (nm) from AFM
low	0.74	17 ± 1.2	18 ± 1.6
medium	0.74	18 ± 1.2	20 ± 3.5
high	0.81	18 ± 1.1	19 ± 2.0

matrix phase, has been previously determined by wide-angle X-ray scattering (WAXS).[12] Values for L_m in annealed polyethylene have been previously determined by SAXS to be between 10 and 30 nm depending upon processing conditions.[28,31] Our values obtained for L_m by SANS and AFM compare well to those values and are presented in Table 2. The similarity in the results we determine for lamellae thickness suggests that, despite the fact that AFM is inherently a surface technique and SANS is a bulk approach, we are studying similar microstructures with both. Additionally, this implies that morphology development mechanisms at the surface are similar to those of the bulk and that results from AFM measurements can be extended to interpretation of bulk experiments.

Turning our analysis to the voids themselves, Figure 3 displays both height and phase images of 36% medium-structure carbon black in hPE at increasing magnification, allowing for close inspection of composite microstructure, including the void phase. In Figure 3a,b, phase imaging clearly shows the interface between polyethylene lamellae and carbon black aggregates, but voids are not directly apparent. Inspection of the complementary height image, however, reveals distinct discontinuities at these locations. This free space at the carbon black−polyethylene interface, revealed by the comparison of height and phase images, is the void phase. Figure 3c also contains cross sections of the scan that enable size measurements to be taken. The mean void size in this scan, determined by averaging 12 such measurements at 30° increments in order to average out orientational dependence, is approximately 70 nm, within the range measured by SANS for the carbon black of medium structure. Although the determination of void sizes by AFM and SANS is made in two and three dimensions by fundamentally different methods, this comparison demonstrates that surface and bulk morphology are of similar length scales.

Figure 4 illustrates several examples, marked by arrows in Figure 3c, of void formation at the carbon

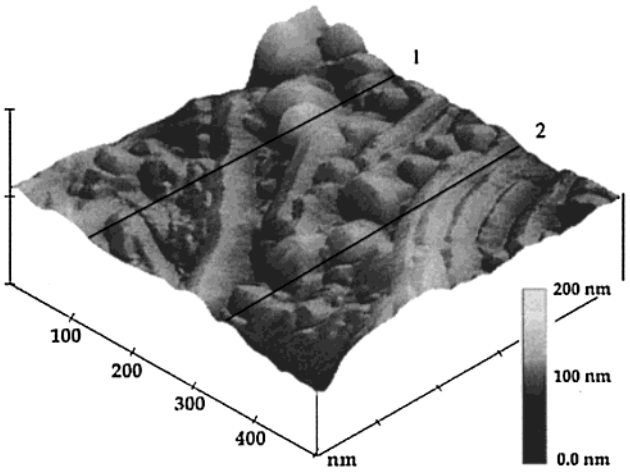

Figure 4. Surface plot showing Figure 3c in greater detail. Transverse lines on the image also correspond to those on Figure 3c.

black−polyethylene interface. In this image both the stacked lamellar geometry of polyethylene and the aggregate or "beads on a string" morphology of carbon black are evident. In this case, it appears that the crystalline polymer has excluded carbon black during the crystallization process and dewetted the surface at a contact point between primary carbon black particles, generating voids.

In Figure 5 we observe variations of the mechanism through which crystallization appears to induce void formation. Figure 5a shows lamellae originating and running perpendicular to the carbon black surface, indicating that polyethylene adsorbed to particle surfaces, known as bound polymer or carbon gel,[32,33] does not fully desorb upon crystallization and therefore influences composite morphology development. While polyethylene remains bound to the carbon black surface at particular locations, the growth of higher density polymer lamellae results in dewetting at other interfacial locations.

When many carbon black aggregates are present in the same area, as in Figure 5b, and lamellar propagation occurs in multiple directions from particle surfaces, their growth may eventually become hindered at intersection points or upon encountering another aggregate. At these points, once again, voids appear to form as polyethylene dewetts from the carbon black surface. Similarly, Figure 5c displays a large void between

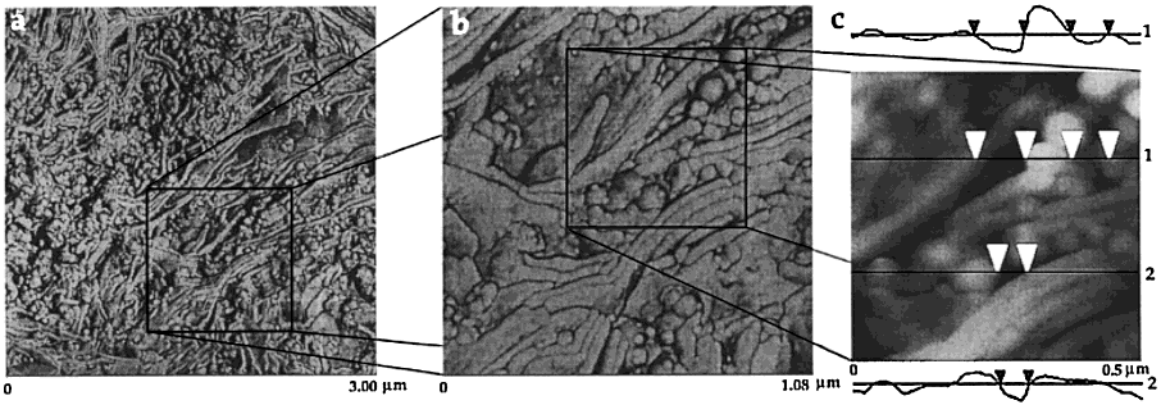

Figure 3. (a, b) Phase images of a 36% medium structure carbon black-filled polyethylene composite. Magnification is increased from (a) 3 μm to (b) 1.08 μm. A corresponding height image (c) is also shown with cross sections. Arrows indicate the width of voids along the transverse line drawn on the image as well as the cross section plots at the top and bottom.

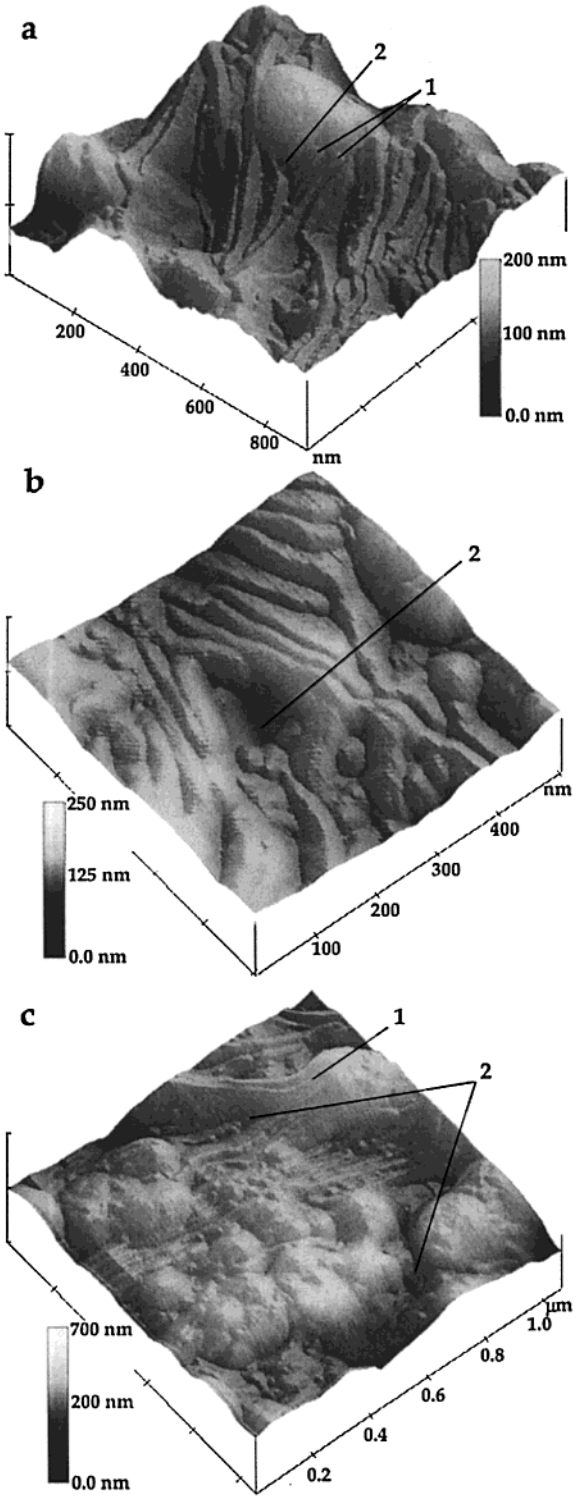

Figure 5. AFM images of local conductive composite morphology demonstrating the connection of lamellae to carbon black particle surfaces (1) and the formation of a void between adjacent carbon black aggregates (2).

adjacent excluded carbon black aggregates perpendicular to the local direction of lamellar growth.

These hypotheses for void formation can be interpreted in the context of a phenomenological scaling argument developed from SANS results and presented in a previous paper.[12] It was shown that void volume fraction (ϕ_3) can be predicted with knowledge of carbon black structure (*DBP*), carbon black volume fraction (ϕ_2), polymer weight percent crystallinity (χ), and volume

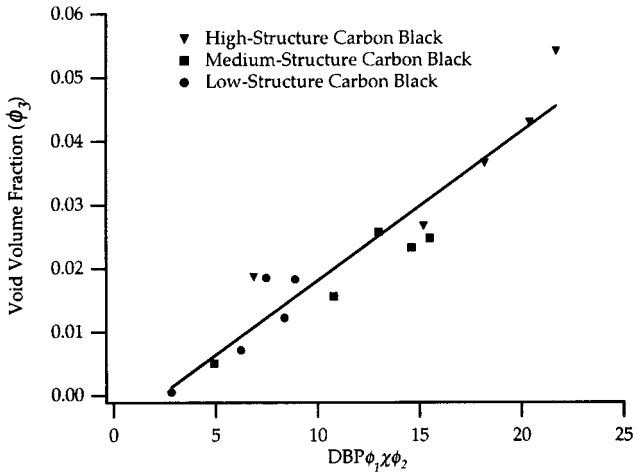

Figure 6. Void content plotted against $DBP\phi_1\chi\phi_2$. Annealed (▼, ■, ●) and quenched (▽, □, ○) composites are shown.

fraction (ϕ_1). Mathematically, this argument was presented as

$$\phi_3 \propto DBP\phi_1\chi\phi_2 \tag{1}$$

and is valid at room temperature. Figure 6 is the linear plot that results when the experimentally determined void volume fraction is plotted against that predicted by eq 1 for the same composites studied by AFM in this work. This indicates that the correct origins of void formation were identified and that void content is proportional to the carbon black−polyethylene interfacial surface area present. AFM images presented here, however, allow for a more thorough understanding of the void formation mechanisms suggested by these SANS results. The atomic force micrographs presented in Figures 3−5 show that voids do form at the carbon black−polyethylene interface. Furthermore, voids appear primarily at points where polyethylene lamellae either nucleate at or tangentially contact a carbon black aggregate. These observations, coupled with SANS results that correlate the appearance of voids with the onset of matrix crystallization, lead to the conclusion that void formation as a method of stress relief is correct. The disappearance of voids in the melt is also accounted for by diffusion and readsorption of polymer chains to the carbon black surface, resulting in uniform particle coverage. Finally, the linear increase in void volume fraction with carbon black content is readily explained as the result of increased matrix−filler interfacial surface area where voids form.

The increase in void volume fraction with carbon black structure observed in the previous work is also accounted for by void formation at the interface. More highly structured carbon blacks, characterized by a higher *DBP* number, possess a greater amount of surface area, thus providing an opportunity for the formation of more voids. Void size, however, has also been shown to increase with structure (Table 1), suggesting that it may be individual void volume and not number contributing to the increase in void volume fraction with carbon black structure. Because the carbon blacks used in these experiments increase in primary particle and aggregate size along with structure, the corresponding increase in void volume fraction is likely a combination of both possibilities. To decouple the individual effects of particle size and structure, it would be necessary to repeat these experiments with compos-

ites formulated with uniformly sized carbon black over a range of structures and uniformly structured carbon black over a range of sizes.

Conclusions

While previous small-angle scattering based experiments have identified and quantified voids within bulk carbon black-filled polyethylene composites, the local morphology of voids, and conductive composites in general, has remained unknown. We have demonstrated that AFM can be used to study conductive composite bulk morphology with excellent resolution. This technique allows identification of voids through a comparison of complementary height and phase images. With this technique, it has been determined, as previously hypothesized, that voids form at the carbon black−polyethylene interface. The evidence presented also suggests that voids form as a mechanism of relieving stresses generated during polyethylene crystallization and can be attributed primarily to polyethylene dewetting at the carbon black particle surface.

Acknowledgment. We acknowledge the support of the National Institute of Standards and Technology, U.S. Department of Commerce, in providing the neutron facilities used in this work. This material is supported by the National Science Foundation under Agreement DMR-9423101.

References and Notes

(1) Wignall, G. D.; Farrar, N. R.; Morris, S. *J. Mater. Sci.* **1990**, *25*, 69−75.
(2) Breuer, O.; Tchoudakov, R.; Narkis, M.; Siegmann, A. *J. Appl. Polym. Sci.* **1997**, *64*, 1097−1106.
(3) Salome, L.; Carmona, F. *Carbon* **1991**, *29*, 599−604.
(4) Hjelm, R. P.; Seeger, P. A.; Wampler, W. A. *Polym. Polym. Compos.* **1993**, *1*, 53A−69A.
(5) Carmona, F. *Physica A* **1989**, *157*, 461−469.
(6) Beaucage, G.; Rane, S.; Schaefer, D. W.; Long, G.; Fischer, D. *J. Polym. Sci. B* **1999**, *37*, 1105−1119.
(7) Heaney, M. B. *Phys. Rev. B* **1995**, *52*, 12477−12480.
(8) Viswanathan, R.; Heaney, M. B. *Phys. Rev. Lett.* **1995**, *75*, 4433−4436.
(9) Oakes, J. A.; Sandberg, C. L. *IEEE Trans. Ind. Appl.* **1973**, *IA-9*, 462−466.
(10) Doljack, F. A. *IEEE Trans. Comput., Hybrids, Manuf. Technol.* **1981**, *CHMT-4*, 372−378.
(11) Marr, D. W. M.; Wartenberg, M.; Schwartz, K. B.; Agamalian, M. M.; Wignall, G. D. *Macromolecules* **1997**, *30*, 2120−2124.
(12) Oakey, J.; Marr, D. W. M.; Schwartz, K. B.; Wartenberg, M. *Macromolecules* **1999**, *32*, 5399−5404.
(13) Pfau, A.; Janke, A.; Heckman, W. *Surf. Interface Anal.* **1999**, *27*, 410−417.
(14) Keita, B.; Nadjo, L.; Gachard, E.; Remita, H.; Khatouri, J.; Belloni, J. *New J. Chem.* **1997**, *21*, 851−855.
(15) Maas, S.; Gronski, W. *Kautschuk Gummi Kunststoffe* **1994**, *47*, 409.
(16) Vansco, G. J.; Liu, G.; Karger-Kocsis, J.; Varga, J. *Colloid Polym. Sci.* **1997**, *275*, 181−186.
(17) Lee, J.-C.; Nakajima, K.; Ikehara, T.; Nishi, T. *J. Appl. Polym. Sci.* **1996**, *64*, 797−802.
(18) Maas, S.; Gronski, W. *Rubber Chem. Tech.* **1995**, *68*, 652−659.
(19) DACA Instruments, Santa Barbara, CA.
(20) Batiashvili, M. S.; Lomtadze, T. T.; Georkhelidze, N. N. *Int. Polym. Sci. Technol.* **1990**, *17*, T/76−T/77.
(21) Hawkins, W. L. *Polymer Stabilization*; Wiley-Interscience: New York, 1972; p 91.
(22) Holmstrom, A. *Durability of Macromolecular Materials*; American Chemical Society: Washington, DC, 1979; pp 45−62.
(23) Gilroy, H. M. *Durability of Macromolecular Materials*; American Chemical Society: Washington, DC, 1979; pp 63−74.
(24) Wignall, G. D.; Bates, F. S. *J. Appl. Crystallogr.* **1987**, *20*.
(25) Dubner, W. S.; Schultz, J. M.; Wignall, G. D. *J. Appl. Crystallogr.* **1990**, *23*, 469−475.
(26) Magonov, S. N.; Whangbo, M.-H. *Adv. Mater.* **1994**, *6*, 355−371.
(27) Howald, L.; Haefke, H.; Luthi, R.; Meyer, E.; Gerth, G.; Rudin, H.; Guntherodt, H.-J. *Phys. Rev. B* **1994**, *49*, 5651−5656.
(28) Zhou, H.; Wilkes, G. L. *Polymer* **1997**, *38*, 5735−5747.
(29) Stanjek, H.; Niederbudde, E. A.; Hausler, W. *Clay Miner.* **1992**, *27*, 3−19.
(30) Klug, H. P.; Alexander, L. E. *X-ray Diffraction Procedures For Polycrystalline and Amorphous Materials*; John Wiley & Sons: New York, 1954; pp 132−134.
(31) Spells, S. J.; Hill, M. J. *Polymer* **1991**, *32*, 2716−2723.
(32) Kida, N.; Ito, M.; Kaido, H. *J. Appl. Polym. Sci.* **1996**, *61*, 1345−1350.
(33) Leblanc, J. L.; Stragliati, B. *J. Appl. Polym. Sci.* **1997**, *63*, 959−970.
(34) Determined following ASTM Designation D3849-89.

MA0000024